NLO QCD corrections to the B_c-pair hadroproduction

Zi-Qiang Chen,[1,‡] Long-Bin Chen,[1,*] and Cong-Feng Qiao[2,†]
[1]School of Physics and Materials Science, Guangzhou University, Guangzhou 510006, China
[2]School of Physical Sciences, University of Chinese Academy of Science, Yuquan Road 19A, Beijing 100049, China

(Received 15 February 2024; accepted 6 May 2024; published 23 May 2024)

The B_c meson pair, including pairs of pseudoscalar states and vector states, productions in proton-proton collisions are investigated at the next-to-leading order (NLO) accuracy in the nonrelativistic quantum chromodynamics factorization formalism. The corresponding cross sections at the Large Hadron Collider (LHC) with $\sqrt{s} = 14$ TeV are evaluated. Numerical results indicate that the NLO corrections are substantial, and even dominate over the leading order contributions. Considering the predicted cross sections are sizable, the B_c-pair production is expected to be observable at the high-luminosity LHC experiment.

DOI: 10.1103/PhysRevD.109.096032

I. INTRODUCTION

As a multiscale system consisting of two heavy quarks, heavy quarkonium presents an ideal laboratory for testing the interplay between perturbative and nonperturbative quantum chromodynamics (QCD) within a controlled environment. Due to the large mass of heavy quark, quarkonium production process is assumed to be factorizable into two steps. First, a heavy quark-antiquark pair whose invariant mass near the bound-state mass is produced perturbatively, then the pair hadronizes into a quarkonium state nonperturbatively. The nonrelativistic QCD (NRQCD) factorization formalism, which proposed by Bodwin, Braaten, and Lepage [1], provides a solid foundation for the theoretical study of quarkonium production. In NRQCD factorization approach, the nonperturbative hadronization effects are encoded into the long distance matrix elements (LDMEs), which are sorted in powers of the relative velocity v of the heavy quarks in the bound state. Although the quarkonium production has been extensively investigated at various colliders, the existing researches are still not sufficient to pin down the color-octet (CO) LDMEs (see, for example Refs. [2,3] for a review).

Over the past two decades, there has been increasing interest in quarkonium-pair hadroproduction [4–32] initiated in Ref. [33], as it provides a sensitive test for NRQCD factorization formalism. Due to the high reconstruction efficiency of J/ψ meson, most researches focus on J/ψ-pair production, for which, the contributions of double $c\bar{c}({}^3S_1^{[1]})$ and double $c\bar{c}({}^1S_0^{[8]})$ intermediate states are calculated up to next-to-leading order (NLO) QCD accuracy [21,32]. Nevertheless, there are many challenges in understanding the underlying production mechanism. First, the full NRQCD prediction requires to include the contributions of all possible pairing of $c\bar{c}({}^1S_0^{[8]})$, $c\bar{c}({}^3S_1^{[1,8]})$, and $c\bar{c}({}^3P_J^{[1,8]})$ intermediate states; while the higher-order calculations to these processes are hard to proceed, especially for double $c\bar{c}({}^3P_J^{[1,8]})$ channel [34]. Second, the results of Refs. [21,32] indicate that the NLO corrections may dominant over the leading-order (LO) contributions, which exhibits poor perturbative convergence—one may worry that the calculation at NLO is not accurate enough to make a reliable prediction. Third, the J/ψ-pair hadroproduction may serve as a probe to double parton scattering (DPS) mechanism [17]; while current researches are inadequate to draw any concrete conclusion, since the predictions to the single parton scattering (SPS) contribution are fraught with uncertainties as well.

As the Large Hadron Collider (LHC) may transit to its high luminosity operation in 2029 and beyond, more interesting processes, like the B_c-pair hadroproduction, can be measured with high accuracy. Compared with J/ψ-pair hadroproduction, the production mechanism of B_c-pair hadroproduction is much simpler. Both the DPS and CO contributions are expected to be small in comparison with the traditional color-singlet SPS contribution, due to the fact that the B_c meson needs to be produced in accompany with an additional $b\bar{c}$ pair. Hence, the B_c-pair

*Corresponding author: chenlb@gzhu.edu.cn
†Corresponding author: qiaocf@ucas.ac.cn
‡chenziqiang13@mails.ucas.ac.cn

hadroproduction provides a complementary approach to clarifying the puzzles in J/ψ-pair hadroproduction, and more clear conclusions can be expected due to its simple production mechanism. In Refs. [13,15], the LO calculation of B_c-pair hadroproduction is performed in the NRQCD factorization framework, and in Ref. [22], the relativistic correction is carried out by using the relativistic quark model approach. Considering the fact that the NLO QCD corrections to quarkonium-pair production processes are normally significant [21,32], in this work, we calculate the NLO QCD corrections to B_c-pair hadroproduction. Various of S-wave B_c states, including configurations of $B_c^+ + B_c^-$, $B_c^+ + B_c^{*-}$,[1] and $B_c^{*+} + B_c^{*-}$, are taken into account. Note, here after for simplicity, B_c represents for both pseudoscalar B_c and vector B_c^*, the latter may overwhelmingly decay to the pseudoscalar state, unless specifically mentioned.

The rest of the paper is organized as follows. In Sec. II, we present the LO calculation of B_c-pair production in proton-proton collisions. In Sec. III, some technical details in the calculation of NLO corrections are given. In Sec. IV, the numerical evaluation for concerned processes is performed at NLO QCD accuracy. The last section is a summary and conclusions.

II. THE LO CROSS SECTIONS

At the LO in α_s, B_c-pair hadronproduction receives contributions from two partonic processes, namely the gg-induced process

$$g(p_1) + g(p_2) \to B_c^+(k_1) + B_c^-(k_2), \tag{1}$$

and the $q\bar{q}$-induced process

$$q(p_1) + \bar{q}(p_2) \to B_c^+(k_1) + B_c^-(k_2), \tag{2}$$

whose Feynman Diagrams are shown in Fig. 1. Since the $q\bar{q}$-induced process is suppressed by quark parton distribution functions (PDFs), it was missed by previous LO studies [13,15,22]. While at NLO, to eliminate the collinear singularities of the real emission process $g + q(\bar{q}) \to B_c^+ + B_c^- + q(\bar{q})$, the $q\bar{q}$-induced process should be convoluted with the scale dependent PDFs. Hence, for a thorough study, both gg- and $q\bar{q}$-induced processes should be taken into account. In fact, our numerical results show that at LO the contribution of $q\bar{q}$-induced process may reach 10% in some cases, which is not really negligible.

According to the NRQCD factorization formalism, the LO partonic cross section can be formulated as

[1]The productions of $B_c^+ + B_c^{*-}$ and $B_c^{*+} + B_c^-$ are related by a charge conjugation transformation. Their cross sections are exactly the same.

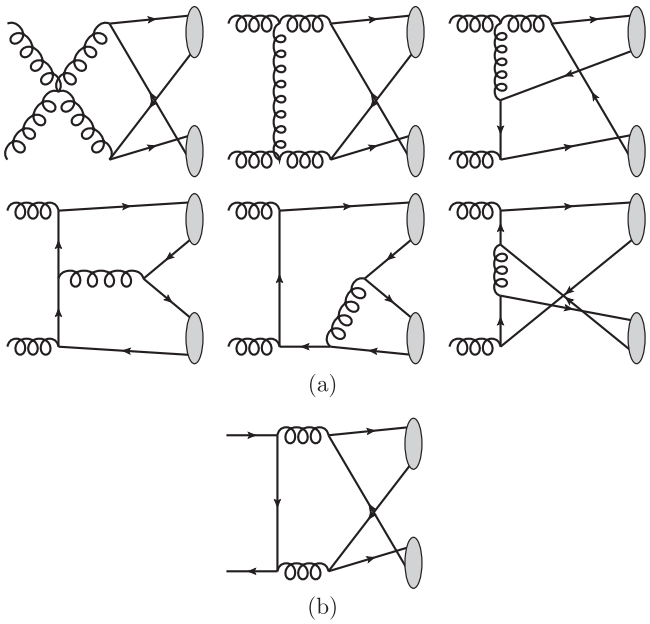

FIG. 1. The typical tree-level Feynman diagrams for (a) gg-induced process, and (b) $q\bar{q}$-induced process. The remaining diagrams can be obtained by reversing the quark lines, or interchanging the initial gluons.

$$d\hat{\sigma}_{\rm LO}^{i+j\to B_c^+ + B_c^-} = \frac{|\Psi(0)|^4}{2s}\overline{\sum}\left|\mathcal{M}_{\rm tree}^{i+j\to[b\bar{c}]+[\bar{b}c]}\right|^2 d{\rm PS}_2, \tag{3}$$

where $\Psi(0)$ is the wave function of B_c meson at the origin, $s = (p_1 + p_2)^2$ is the center-of-mass energy squared of the colliding partons i and j, $\overline{\sum}$ sums (averages) over the polarizations and colors of the final (initial) state particles, $\mathcal{M}_{\rm tree}^{i+j\to[b\bar{c}]+[\bar{b}c]}$ is the corresponding LO partonic amplitude, and $d{\rm PS}_2$ stands for the two-body phase space.

The partonic amplitude can be computed by using the covariant projection operator method. At the leading order of the relative velocity expansion, it is legitimate to take $m_{B_c} = m_b + m_c$, $p_{B_c} = p_c + p_b = (1 + \frac{m_c}{m_b})p_b$, where m_{B_c} and p_{B_c} denote the mass and momentum of the B_c meson, respectively. The spin and color projection operators take the form,

$$\Pi(n) = \frac{1}{2\sqrt{m_{B_c}}}\varepsilon(n)(\not{p}_{B_c} + m_{B_c}) \otimes \frac{1_c}{\sqrt{N_c}}, \tag{4}$$

where $\varepsilon(^1S_0) = \gamma_5$, $\varepsilon(^3S_1) = \not{\epsilon}$, and ϵ represents the polarization vector of B_c^* meson. The 1_c stands for the unit color matrix, and $N_c = 3$ is the number of colors in QCD.

The LO calculation is straightforward, and the analytic expressions for $\overline{\sum}|\mathcal{M}|^2$ are pretty simple. By introducing the dimensionless variables $\hat{s} = (p_1 + p_2)^2/m_{B_c}^2$, $\hat{v} = -(p_1 - p_2)\cdot(k_1 - k_2)/m_{B_c}^2$, $\hat{w} = \sqrt{\hat{s}^2 - \hat{v}^2}$, and $r = m_b/(m_b + m_c)$, we have

$$\overline{\sum}\left|\mathcal{M}_{\text{tree}}^{g+g\to{}^1S_0+{}^1S_0}\right|^2=\frac{g_s^8}{m_{B_c}^6r^4(1-r)^4}\left[\frac{157}{36\hat{s}^4}-\frac{374}{9\hat{s}^3\hat{w}^2}+\frac{22}{27\hat{s}^3}+\frac{32\hat{s}^2}{81\hat{w}^8}+\frac{968}{9\hat{s}^2\hat{w}^4}-\frac{241}{27\hat{s}^2\hat{w}^2}+\frac{4}{81\hat{s}^2}-\frac{16\hat{s}}{9\hat{w}^6}+\frac{860}{27\hat{s}\hat{w}^4}-\frac{4}{9\hat{s}\hat{w}^2}\right.$$
$$-\frac{352}{27\hat{w}^6}+\frac{178}{81\hat{w}^4}+\frac{1}{r(1-r)}\left(\frac{11\hat{w}^2}{24\hat{s}^5}+\frac{\hat{w}^2}{18\hat{s}^4}-\frac{170}{27\hat{s}^4}+\frac{844}{27\hat{s}^3\hat{w}^2}-\frac{731}{648\hat{s}^3}-\frac{1408}{27\hat{s}^2\hat{w}^4}+\frac{613}{81\hat{s}^2\hat{w}^2}-\frac{1}{18\hat{s}^2}\right.$$
$$\left.+\frac{40\hat{s}}{81\hat{w}^6}-\frac{1340}{81\hat{s}\hat{w}^4}+\frac{17}{36\hat{s}\hat{w}^2}+\frac{256}{81\hat{w}^6}-\frac{11}{9\hat{w}^4}\right)+\frac{1}{r^2(1-r)^2}\left(\frac{\hat{w}^4}{64\hat{s}^6}-\frac{17\hat{w}^2}{72\hat{s}^5}-\frac{\hat{w}^2}{32\hat{s}^4}+\frac{257}{162\hat{s}^4}-\frac{416}{81\hat{s}^3\hat{w}^2}\right.$$
$$\left.\left.+\frac{13}{36\hat{s}^3}+\frac{512}{81\hat{s}^2\hat{w}^4}-\frac{13}{9\hat{s}^2\hat{w}^2}+\frac{1}{64\hat{s}^2}+\frac{160}{81\hat{s}\hat{w}^4}-\frac{1}{8\hat{s}\hat{w}^2}+\frac{41}{162\hat{w}^4}\right)\right],\tag{5}$$

$$\overline{\sum}\left|\mathcal{M}_{\text{tree}}^{g+g\to{}^1S_0+{}^3S_1}\right|^2=\frac{g_s^8(1-2r)^2}{m_{B_c}^6r^6(1-r)^6}\left[-\frac{\hat{w}^2}{64\hat{s}^4}+\frac{31}{648\hat{s}^3}+\frac{1}{18\hat{s}^2\hat{w}^2}+\frac{1}{64\hat{s}^2}+\frac{1}{648\hat{s}\hat{w}^2}-\frac{41}{162\hat{w}^4}\right],\tag{6}$$

$$\overline{\sum}\left|\mathcal{M}_{\text{tree}}^{g+g\to{}^3S_1+{}^3S_1}\right|^2=\frac{g_s^8}{m_{B_c}^6r^4(1-r)^4}\left[\frac{32\hat{s}^4}{81\hat{w}^8}+\frac{157}{12\hat{s}^4}-\frac{374}{3\hat{s}^3\hat{w}^2}-\frac{143}{81\hat{s}^3}+\frac{32\hat{s}^2}{27\hat{w}^8}-\frac{32\hat{s}^2}{9\hat{w}^6}+\frac{968}{3\hat{s}^2\hat{w}^4}+\frac{143}{27\hat{s}^2\hat{w}^2}+\frac{4}{81\hat{s}^2}+\frac{80\hat{s}}{81\hat{w}^6}\right.$$
$$-\frac{236}{27\hat{s}\hat{w}^4}+\frac{109}{81\hat{s}\hat{w}^2}-\frac{352}{9\hat{w}^6}+\frac{92}{27\hat{w}^4}+\frac{1}{r(1-r)}\left(\frac{11\hat{w}^2}{8\hat{s}^5}+\frac{\hat{w}^2}{18\hat{s}^4}-\frac{170}{9\hat{s}^4}+\frac{844}{9\hat{s}^3\hat{w}^2}-\frac{475}{216\hat{s}^3}\right.$$
$$+\frac{64\hat{s}^2}{81\hat{w}^6}-\frac{1408}{9\hat{s}^2\hat{w}^4}+\frac{1021}{81\hat{s}^2\hat{w}^2}-\frac{1}{18\hat{s}^2}+\frac{40\hat{s}}{27\hat{w}^6}-\frac{2\hat{s}}{9\hat{w}^4}-\frac{1972}{81\hat{s}\hat{w}^4}+\frac{275}{324\hat{s}\hat{w}^2}+\frac{256}{27\hat{w}^6}-\frac{61}{27\hat{w}^4}\Big)$$
$$+\frac{1}{r^2(1-r)^2}\left(\frac{3\hat{w}^4}{64\hat{s}^6}-\frac{17\hat{w}^2}{24\hat{s}^5}-\frac{\hat{w}^2}{8\hat{s}^4}+\frac{257}{54\hat{s}^4}-\frac{416}{27\hat{s}^3\hat{w}^2}+\frac{191}{162\hat{s}^3}+\frac{512}{27\hat{s}^2\hat{w}^4}-\frac{38}{9\hat{s}^2\hat{w}^2}+\frac{5}{64\hat{s}^2}\right.$$
$$\left.\left.+\frac{160}{27\hat{s}\hat{w}^4}-\frac{241}{648\hat{s}\hat{w}^2}+\frac{41}{162\hat{w}^4}\right)\right],\tag{7}$$

for gg-induced process, and

$$\overline{\sum}\left|\mathcal{M}_{\text{tree}}^{q+\bar{q}\to{}^1S_0+{}^1S_0}\right|^2=\frac{g_s^8}{m_{B_c}^6r^6(1-r)^6}\left[-\frac{2\hat{v}^4}{243\hat{s}^6}-\frac{8\hat{v}^2}{243\hat{s}^5}+\frac{2\hat{v}^2}{243\hat{s}^4}\right],\tag{8}$$

$$\overline{\sum}\left|\mathcal{M}_{\text{tree}}^{q+\bar{q}\to{}^1S_0+{}^3S_1}\right|^2=\frac{g_s^8(1-2r)^2}{m_{B_c}^6r^6(1-r)^6}\left[-\frac{2\hat{v}^2}{243\hat{s}^4}+\frac{8}{243\hat{s}^3}+\frac{2}{243\hat{s}^2}\right],\tag{9}$$

$$\overline{\sum}\left|\mathcal{M}_{\text{tree}}^{q+\bar{q}\to{}^3S_1+{}^3S_1}\right|^2=\frac{g_s^8}{m_{B_c}^6r^6(1-r)^6}\left[-\frac{2\hat{v}^4}{81\hat{s}^6}-\frac{8\hat{v}^2}{81\hat{s}^5}+\frac{2\hat{v}^2}{243\hat{s}^4}+\frac{16}{243\hat{s}^3}+\frac{4}{243\hat{s}^2}\right],\tag{10}$$

for $q\bar{q}$ induce process. Here, the strong coupling constant is denoted by g_s. Note, for charmonium-pair production, the processes $g+g\to J/\psi+\eta_c$ and $q+\bar{q}\to J/\psi+\eta_c$ are forbidden in the color-singlet model, due to the requirement of charge-parity C conservation. For the same reason, the amplitudes for $B_c^+ + B_c^{*-}$ production [Eqs. (6) and (9)] vanish in the limit $m_b\to m_c$.

III. THE NLO QCD CORRECTIONS

The NLO QCD corrections to B_c-pair hadroproduction include virtual and real corrections, which are outlined in Secs. III A and III B, respectively.

A. The virtual corrections

The virtual corrections comprise about 1300 one-loop diagrams for the gg and about 100 diagrams for the $q\bar{q}$-induced process, the most complicated being the 38 and 8 hexagons for the respective channels, as shown in Fig. 2. The contribution of virtual corrections can be formulated as

$$d\hat{\sigma}_{\text{virtual}}=\frac{|\Psi(0)|^4}{2s}\overline{\sum}2\text{Re}(\mathcal{M}_{1\text{-loop}}\mathcal{M}_{\text{tree}}^*)d\text{PS}_2.\tag{11}$$

Here, the interference term $\text{Re}(\mathcal{M}_{1\text{-loop}}\mathcal{M}_{\text{tree}}^*)$ contains both ultraviolet (UV) and infrared (IR) singularities.

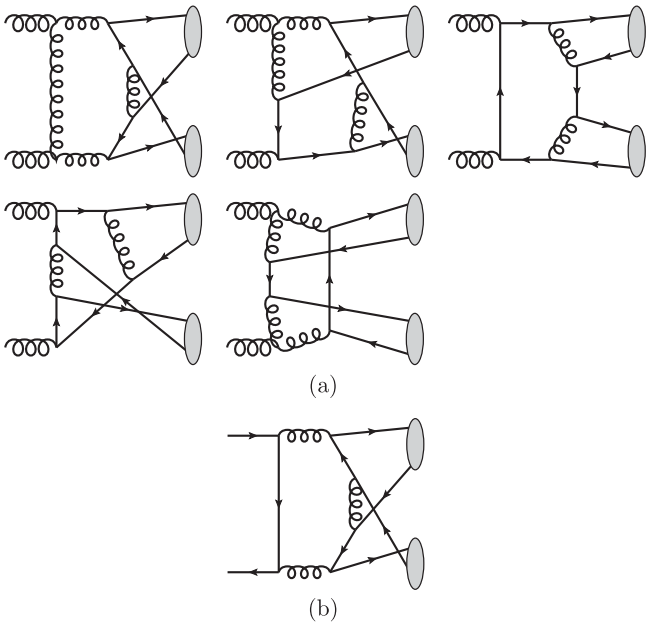

FIG. 2. The typical hexagon diagrams for (a) gg-induced process and (b) $q\bar{q}$-induced process. The remaining diagrams can be obtained by reversing the quark lines, or interchanging the initial gluons.

The conventional dimensional regularization with $D = 4 - 2\epsilon$ is employed to regularize them. The method proposed in Refs. [35,36] is used to deal with the D-dimensional γ_5 trace.

The UV singularities, which are contained in self-energy and triangle diagrams, are canceled by corresponding counterterm diagrams. The relevant renormalization constants include Z_2, Z_m, Z_3, Z_l, and Z_g, corresponding to heavy quark field, heavy quark mass, gluon field, light quark field, and strong coupling constant, respectively. We define Z_2, Z_m, Z_3, and Z_l in the on shell (OS) scheme, Z_g in the modified minimal-subtraction ($\overline{\text{MS}}$) scheme. The counterterms are

$$\begin{aligned}
\delta Z_2^{\text{OS}} &= -C_F \frac{\alpha_s}{4\pi}\left[\frac{1}{\epsilon_{\text{UV}}} + \frac{2}{\epsilon_{\text{IR}}} - 3\gamma_E + 3\ln\frac{4\pi\mu^2}{m_Q^2} + 4\right],\\
\delta Z_m^{\text{OS}} &= -3C_F \frac{\alpha_s}{4\pi}\left[\frac{1}{\epsilon_{\text{UV}}} - \gamma_E + \ln\frac{4\pi\mu^2}{m_Q^2} + \frac{4}{3}\right],\\
\delta Z_l^{\text{OS}} &= -C_F \frac{\alpha_s}{4\pi}\left[\frac{1}{\epsilon_{\text{UV}}} - \frac{1}{\epsilon_{\text{IR}}}\right],\\
\delta Z_3^{\text{OS}} &= \left(\beta_0^{\text{light}} - 2C_A\right)\frac{\alpha_s}{4\pi}\left[\frac{1}{\epsilon_{\text{UV}}} - \frac{1}{\epsilon_{\text{IR}}}\right]\\
&\quad - \sum_{Q=b,c}\frac{4}{3}T_F\frac{\alpha_s}{4\pi}\left[\frac{1}{\epsilon_{\text{UV}}} - \gamma_E + \ln\frac{4\pi\mu^2}{m_Q^2}\right],\\
\delta Z_g^{\overline{\text{MS}}} &= -\frac{\beta_0}{2}\frac{\alpha_s}{4\pi}\left[\frac{1}{\epsilon_{\text{UV}}} - \gamma_E + \ln(4\pi)\right]. \qquad (12)
\end{aligned}$$

Here, μ is the renormalization scale, γ_E is the Euler's constant, m_Q stands for m_b and m_c accordingly, $\beta_0^{(\text{light})} = (11/3)C_A - (4/3)T_F n_f^{(\text{light})}$ is the one-loop coefficient of QCD beta function with $n_f = 5$ being the number of active quarks, $n_f^{\text{light}} = 3$ is the number of light quarks, $C_A = 3$, $C_F = 4/3$, and $T_F = 1/2$ are color factors.

The IR singularities in virtual corrections can be classified into two groups; the final-state-related singularities and the initial-state-related ones. The former arise from diagrams where one final-state particle exchanges a soft gluon with another on shell particle. This type of singularities cancel each other as expected [1,37,38]. The initial-state-related singularities stem from diagrams where the two initial state partons are connected by a soft gluon, or where one initial state parton is attached by a collinear gluon. According to the Kinoshita-Lee-Nauenberg theorem [39,40], parts of initial-state-related singularities are canceled by the real corrections, and the remainings are eliminated by introducing the scale dependent PDFs.

The Coulomb singularities arise when two heavy quarks, which move with a small relative velocity, exchange a soft gluon between them. For each B_c meson, since we set $p_c = \frac{m_c}{m_b} p_b$ before the calculation of Feynman integrals, the corresponding Coulomb singularities are absent in the dimensional regularization [41]. While there is another type of Coulomb singularities: in the threshold region where $s \sim 4m_{B_c}^2$, the valence quark of B_c^+ moves with a small velocity relative to the valence quark of B_c^-. In this case, the Coulomb singularities appear as $1/\sqrt{s - 4m_{B_c}^2}$ terms. We find that these terms vanish after summing up all one-loop diagrams.

B. The real corrections

The real corrections are induced by the partonic processes,

$$g(p_1) + g(p_2) \to B_c^+(k_1) + B_c^-(k_2) + g(p_3), \qquad (13)$$

$$q(p_1) + \bar{q}(p_2) \to B_c^+(k_1) + B_c^-(k_2) + g(p_3), \qquad (14)$$

$$g(p_1) + q(\bar{q})(p_2) \to B_c^+(k_1) + B_c^-(k_2) + q(\bar{q})(p_3). \qquad (15)$$

Here, processes (13) and (14) are the gluon bremsstrahlung corrections to corresponding LO processes. Process (15) indicates a new production channel, namely the gluon-quark scattering. The typical Feynman diagrams for processes (13) and (14) are shown in Fig. 3. The diagrams for process (15) can be obtained through crossing.

In the calculation of real corrections, the Catani-Seymour (CS) dipole subtraction method [42,43] is adopted to handle the IR singularities. The general idea of this method is to rewrite the NLO corrections as

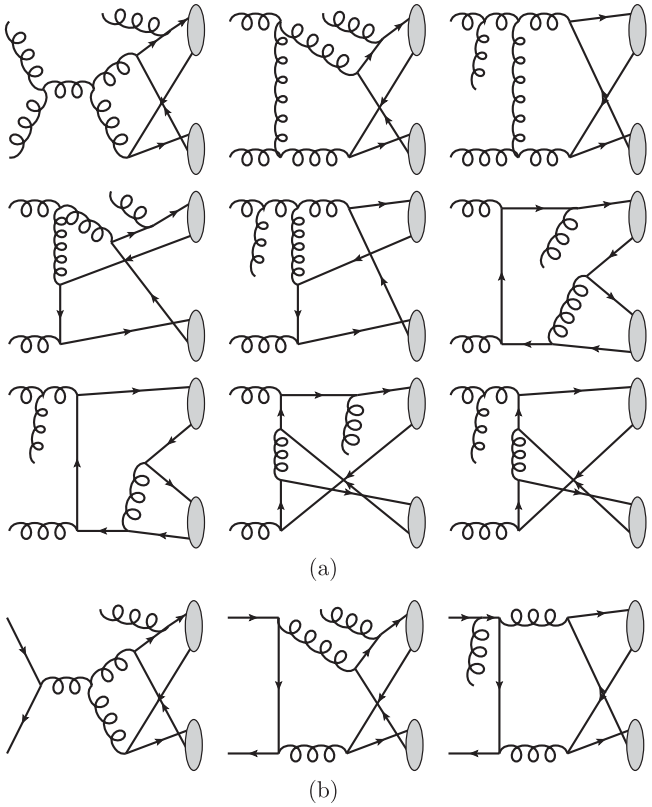

FIG. 3. Typical Feynman diagrams for (a) $g+g\to B_c^+ + B_c^- + g$; (b) $q+\bar{q}\to B_c^+ + B_c^- + g$. The diagrams for $g+q(\bar{q})\to B_c^+ + B_c^- + q(\bar{q})$ can be obtained through crossing.

$$\hat{\sigma}_{\rm NLO} = \int_{\text{3-body}} \left[d\hat{\sigma}_{\rm real} - d\hat{\sigma}_A\right] + \int_{\text{2-body}} \left[d\hat{\sigma}_{\rm virtual} + d\hat{\sigma}_C + \int_{\text{1-body}} d\hat{\sigma}_A\right]. \quad (16)$$

Here, $d\hat{\sigma}_A$ is an auxiliary dipole subtraction term which possesses the same pointwise singular behavior as $d\hat{\sigma}_{\rm real}$, $d\hat{\sigma}_C$ is the collinear subtraction term which originates from the renormalization of PDFs. As $d\hat{\sigma}_A$ acts as a local counter term for $d\hat{\sigma}_{\rm real}$, the first integral of Eq. (16) is nonsingular at every points of phase space, and can be evaluated numerically in four dimensions. On the other hand, the integration of $d\hat{\sigma}_A$ over one-body subspace, i.e., the $\int_{\text{1-body}} d\hat{\sigma}_A$, can be carried out analytically in D dimensions. As a result, and the IR singularities in real corrections appear as pole terms of $1/\epsilon^n$. After adding up $\int_{\text{1-body}} d\hat{\sigma}_A$, $d\hat{\sigma}_{\rm virtual}$ and $d\hat{\sigma}_C$, all IR singularities are eliminated as expected.

The dipole subtraction term $d\hat{\sigma}_A$ can be constructed term by term according to all possible emitter-spectator pairs. While in our case, the contributions of final-state-emission diagrams cancel each other [1,37,38]. Hence, only the dipoles where both emitter and spectator are in the initial state need to be taken into account. Following the implementation of Ref. [42], the $d\hat{\sigma}_A$ is constructed as

$$d\hat{\sigma}_A^{1+2\to[b\bar{c}]+[\bar{b}c]+3} = \frac{1}{2p_1\cdot p_2}\left\{\frac{g_s^2}{p_1\cdot p_3}\frac{P_{11'}(x)}{x}\overline{\sum}\left|\mathcal{M}_{\rm tree}^{1'+2\to[b\bar{c}]+[\bar{b}c]}(\tilde{p}_1,\tilde{p}_2;\tilde{k}_1,\tilde{k}_2)\right|^2 + \frac{g_s^2}{p_2\cdot p_3}\frac{P_{22'}(x)}{x}\overline{\sum}\left|\mathcal{M}_{\rm tree}^{1+2'\to[b\bar{c}]+[\bar{b}c]}(\tilde{p}_1,\tilde{p}_2;\tilde{k}_1,\tilde{k}_2)\right|^2\right\} d\text{PS}_3, \quad (17)$$

where $x = 1-(p_1\cdot p_3 + p_2\cdot p_3)/(p_1\cdot p_2)$ is the momentum fraction at the collinear limit, $P_{ab}(x)$ is the spin average of the Altarelli-Parisi splitting function, which are of the form

$$P_{qq}(x) = C_F\frac{1+x^2}{1-x}, \quad (18)$$

$$P_{qg}(x) = C_F\frac{1+(1-x)^2}{x}, \quad (19)$$

$$P_{gq}(x) = T_F[1-2x(1-x)], \quad (20)$$

$$P_{gg}(x) = 2C_A\left[\frac{x}{1-x}+\frac{1-x}{x}+x(1-x)\right]. \quad (21)$$

The CS projection, which projects the three-body phase space into the two-body one, is implemented as

$$\text{emitter}:\ \tilde{p}_{1,2} = xp_{1,2}, \quad (22)$$

$$\text{spectator}:\ \tilde{p}_{2,1} = p_{2,1}, \quad (23)$$

$$\text{others}:\ \tilde{k}_{1,2} = k_{1,2} - \frac{2k_{1,2}\cdot(K+\tilde{K})}{(K+\tilde{K})^2}(K+\tilde{K}) + \frac{2k_{1,2}\cdot K}{K^2}\tilde{K}, \quad (24)$$

with $K = p_1+p_2-p_3$ and $\tilde{K} = \tilde{p}_1+\tilde{p}_2$.

For the second term of Eq. (16), we have

$$d\hat{\sigma}_C^{1+2\to[b\bar{c}]+[\bar{b}c]+3}+\int_1 d\hat{\sigma}_A^{1+2\to[b\bar{c}]+[\bar{b}c]+3}=\int_0^1 dx\frac{\alpha_s}{2\pi}\frac{1}{\Gamma(1-\epsilon)}\left(\frac{4\pi\mu^2}{2p_1\cdot p_2}\right)^{\epsilon}\Big[d\hat{\sigma}_{\mathrm{LO}}^{1'+2\to[b\bar{c}]+[\bar{b}c]}V_{11'}(x,p_1,p_2,\mu_F)+d\hat{\sigma}_{\mathrm{LO}}^{1+2'\to[b\bar{c}]+[\bar{b}c]}V_{22'}(x,p_1,p_2,\mu_F)\Big], \tag{25}$$

and according to Ref. [42],

$$V_{qq}(x,p_1,p_2,\mu_F)=\frac{4}{3}(1-x)-\frac{8}{3}(1+x)\ln(1-x)+\frac{8}{3}\ln\frac{\sqrt{2p_1\cdot p_2}}{\mu_F}\left[\frac{1+x^2}{1-x}\right]_+ +\frac{16}{3}\left[\frac{\ln(1-x)}{1-x}\right]_+ +\left(\frac{4}{3}\frac{1}{\epsilon^2}+\frac{2}{\epsilon}-\frac{2}{9}\pi^2\right)\delta(1-x), \tag{26}$$

$$V_{gq}(x,p_1,p_2,\mu_F)=[x^2+(1-x)^2]\left[\ln(1-x)+\ln\frac{\sqrt{2p_1\cdot p_2}}{\mu_F}\right]+x(1-x), \tag{27}$$

$$V_{qg}(x,p_1,p_2,\mu_F)=\frac{8}{3}\frac{1+(1-x)^2}{x}\left[\ln(1-x)+\ln\frac{\sqrt{2p_1\cdot p_2}}{\mu_F}\right]+\frac{4}{3}x, \tag{28}$$

$$V_{gg}(x,p_1,p_2,\mu_F)=12\left[-1+x(1-x)+\frac{1-x}{x}\right]\left[\ln(1-x)+\ln\frac{\sqrt{2p_1\cdot p_2}}{\mu_F}\right]+12\left[\frac{\ln(1-x)}{1-x}\right]_+ +12\left[\frac{1}{1-x}\right]_+\ln\frac{\sqrt{2p_1\cdot p_2}}{\mu_F}+\left[\frac{3}{\epsilon^2}+\left(\frac{11}{2}-\frac{n_f^{\mathrm{light}}}{3}\right)\left(\frac{1}{\epsilon}+2\ln\frac{\sqrt{2p_1\cdot p_2}}{\mu_F}\right)-\frac{\pi^2}{2}\right]\delta(1-x). \tag{29}$$

Here, μ_F is the factorization scale, the '+'-distribution is defined as

$$\int_0^1 dx\, g(x)[f(x)]_+=\int_0^1 dx\,[g(x)-g(1)]f(x). \tag{30}$$

IV. NUMERICAL RESULTS

A. Input parameters

We consider B_c-pair production at the LHC with $\sqrt{s}=14$ TeV. The hadron-level cross sections can be obtained by convoluting the partonic cross sections with the proton PDFs,

$$\begin{aligned}d\sigma^{p+p\to B_c^+ +B_c^- +X}=&\int dx_1dx_2f_g(x_1)f_g(x_2)d\hat{\sigma}^{g+g\to B_c^+ +B_c^- +(g)}\\&+\sum_{q=u,d,s}\int dx_1dx_2\left[f_q(x_1)f_{\bar{q}}(x_2)d\hat{\sigma}^{q+\bar{q}\to B_c^+ +B_c^- +(g)}+f_{\bar{q}}(x_1)f_q(x_2)d\hat{\sigma}^{\bar{q}+q\to B_c^+ +B_c^- +(g)}\right]\\&+\sum_{q=u,d,s,\bar{u},\bar{d},\bar{s}}\int dx_1dx_2\left[f_g(x_1)f_q(x_2)d\hat{\sigma}^{q+g\to B_c^+ +B_c^- +q}+f_q(x_1)f_g(x_2)d\hat{\sigma}^{g+q\to B_c^+ +B_c^- +q}\right].\end{aligned} \tag{31}$$

Here, all partonic cross sections are evaluated at $\mathcal{O}(\alpha_s^5)$ accuracy. In our numerical studies, the CT18 NLO parametrization with $\alpha_s(M_Z)=0.118$ [44] is used for the evaluation of PDFs and α_s. The renormalization and factorization scales are chosen as $\mu_0\le\mu_R=\mu_F\le 2\mu_0$, where the central scale μ_0 is taken to be the half of the summed transverse masses of the two B_c mesons, i.e., $\mu_0=(\sqrt{m_{B_c}^2+p_{\mathrm{T},1}^2}+\sqrt{m_{B_c}^2+p_{\mathrm{T},2}^2})/2$.

Other parameters in numerical evaluation go as follows:

$$m_b=4.60\ \mathrm{GeV},\qquad m_c=1.49\ \mathrm{GeV},\qquad |\Psi(0)|^2=0.174\ \mathrm{GeV}^3. \tag{32}$$

Here, the pole masses of heavy quark are obtained through,

$$m_Q = \bar{m}_Q\left(1 + C_F\frac{\alpha_s(\bar{m}_Q)}{\pi}\right), \tag{33}$$

with the $\overline{\text{MS}}$ masses $\bar{m}_b = 4.18$ GeV and $\bar{m}_c = 1.27$ GeV [45] as input. The B_c wave function at the origin is estimated from the $^1S_0 - {}^3S_1$ splitting [46],

$$|\Psi(0)|^2 = \frac{9m_b m_c}{21\pi\alpha_s}(m_{B_c^*} - m_{B_c}), \tag{34}$$

with the lattice calculation result $m_{B_c^*} - m_{B_c} = 53$ MeV [47] as input.

Due to the finite coverage of detectors, proper kinematic cuts should be imposed on the final state particles. Here we employ two typical sets of cuts, which corresponding to the LHCb [48] and ATLAS [49] acceptance of B_c meson, respectively:

(i) LHCb cuts: $1 \le p_{\mathrm{T},1}, p_{\mathrm{T},2} \le 20$ GeV, $2.0 \le y_1, y_2 \le 4.5$;
(ii) ATLAS cuts: $p_{\mathrm{T},1}, p_{\mathrm{T},2} \ge 13$ GeV, $-2.3 \le y_1, y_2 \le 2.3$;

where $p_{\mathrm{T},i}$ and y_i with $i = 1, 2$ denote the transverse momentum and rapidity of each B_c meson respectively. Note, according to Ref. [50], the CMS acceptance cuts of B_c meson are similar to the ATLAS ones.

B. Integrated cross sections

The LO and NLO cross sections for $B_c^+ + B_c^-$, $B_c^+ + B_c^{*-}$ and $B_c^{*+} + B_c^{*-}$ production with different cuts are shown in Table I, wherein, the central values refer to the results at $\mu_{R/F} = \mu_0$, the superscripts and subscripts corresponding to the results at $\mu_{R/F} = \mu_0/2$ and $\mu_{R/F} = 2\mu_0$, respectively. Besides the total cross sections, the partial cross sections for gg-, $q\bar{q}$-, and $gq(\bar{q})$-induced processes, i.e., the first, second, and third lines of Eq. (31), are presented as well. About Table I, there are some points remarkable which are as follows:

(i) Due to the high-gluon flux at low x, the B_c-pair production at the LHC is dominated by the gg-induced processes as expected. While in some cases, the contributions of other partonic processes are also non-negligible. For example, for $B_c^{*+} + B_c^{*-}$ production with ATLAS cuts, the contribution of $gq(\bar{q})$-induced process reaches 20% level at the NLO.
(ii) Similar to the situation of J/ψ-pair production [21], the NLO corrections here may dominate over the LO contributions, and the theoretical uncertainties induced by energy scale is even larger at NLO than that at the LO. We propose a potential explanation based on the kinematic analysis. We find that the bulk of the cross sections arise from the regime where the invariant mass of the B_c-pair M_{2B_c} is small. At LO, the two-body kinematic forces the B_c mesons to be back to back in the transverse momentum plane, hence the p_{T} cut on each B_c meson lead to a constraint of $M_{2B_c} \ge 2\sqrt{m_{B_c}^2 + p_{T,\min}^2}$. While at NLO, the three body real emission processes are involved. In this case, the B_c-pair can be produced near the mass threshold, i.e., $M_{2B_c} \sim 2m_{B_c}$, as long as the recoil parton possesses large enough transverse momentum. The threshold production effect appearing at the

TABLE I. The LO and NLO integrated cross sections for B_c-pair production at the LHC. The LO results agree with those in Ref. [15] after taking the same inputs.

Channel		LHCb cuts (in nb)		ATLAS cuts (in pb)	
Final state	Initial state	LO	NLO	LO	NLO
$B_c^+ + B_c^-$	gg	$2.39^{+0.07}_{-0.36} \times 10^{-1}$	$5.68^{+1.27}_{-0.83} \times 10^{-1}$	$4.09^{+1.04}_{-0.92} \times 10^{-1}$	$2.99^{+1.89}_{-1.04}$
	$q\bar{q}$	$1.90^{+0.69}_{-0.44} \times 10^{-4}$	$1.75^{-1.55}_{+0.48} \times 10^{-4}$	$4.66^{-1.55}_{-1.11} \times 10^{-3}$	$2.93^{-3.67}_{+1.32} \times 10^{-3}$
	$gq(\bar{q})$	–	$0.16^{+7.75}_{-2.83} \times 10^{-2}$	–	$6.99^{+6.10}_{-3.12} \times 10^{-1}$
	total (pp)	$2.39^{+0.07}_{-0.36} \times 10^{-1}$	$5.70^{+2.05}_{-1.11} \times 10^{-1}$	$4.14^{+1.05}_{-0.93} \times 10^{-1}$	$3.69^{+2.50}_{-1.35}$
$B_c^+ + B_c^{*-}$	gg	$3.43^{+0.27}_{-0.58} \times 10^{-2}$	$8.34^{+2.80}_{-1.56} \times 10^{-2}$	$3.46^{+0.89}_{-0.79} \times 10^{-1}$	$3.20^{-0.09}_{+0.05} \times 10^{-1}$
	$q\bar{q}$	$5.36^{+1.94}_{-1.18} \times 10^{-3}$	$3.22^{-5.92}_{+2.12} \times 10^{-3}$	$2.12^{+0.69}_{-0.50} \times 10^{-2}$	$1.36^{-1.67}_{+0.61} \times 10^{-2}$
	$gq(\bar{q})$	–	$0.68^{+1.83}_{-0.76} \times 10^{-2}$	–	$1.16^{+9.56}_{-3.63} \times 10^{-2}$
	total (pp)	$3.96^{+0.46}_{-0.70} \times 10^{-2}$	$9.34^{+4.04}_{-2.12} \times 10^{-2}$	$3.67^{+0.96}_{-0.84} \times 10^{-1}$	$3.45^{+0.70}_{-0.25} \times 10^{-1}$
$B_c^{*+} + B_c^{*-}$	gg	$4.06^{+0.23}_{-0.65} \times 10^{-1}$	$1.10^{+0.47}_{-0.24}$	$3.00^{+0.78}_{-0.68}$	$10.2^{+5.9}_{-3.1}$
	$q\bar{q}$	$4.17^{+1.51}_{-0.92} \times 10^{-2}$	$1.90^{-5.01}_{+1.85} \times 10^{-2}$	$1.76^{+0.57}_{-0.42} \times 10^{-1}$	$0.66^{-1.65}_{+0.66} \times 10^{-1}$
	$gq(\bar{q})$	–	$1.56^{+2.62}_{-1.16} \times 10^{-1}$	–	$2.62^{+2.70}_{-1.32}$
	total (pp)	$4.48^{+0.38}_{-0.74} \times 10^{-1}$	$1.28^{+0.68}_{-0.34}$	$3.17^{+0.84}_{-0.72}$	$12.8^{+8.4}_{-4.3}$

real corrections accounts for the extraordinary large NLO corrections.

(iii) There are negative cross section problems in $q\bar{q}$- and $gq(\bar{q})$-induced processes. For the former, the partial cross sections become negative when $\mu_{R,F}$ approaching $\mu_0/2$, and the large negative corrections can be traced back to the virtual corrections. For the latter, the partial cross sections become negative when $\mu_{R,F}$ approaching $2\mu_0$, and the large negative corrections can be traced back to the over-subtraction of collinear singularities inside the PDFs [51]. Since the contributions of these two processes are not dominant, the total (pp) cross sections keep positive. Hence, in our calculations, no additional treatment is applied to cure the negative cross section problems.

Since B_c^* almost all decays to B_c, a prediction on B_c-pair candidates should sum over all possible final states. By introducing the final-state-summed cross section as $\sigma^{\rm FSS} = \sigma^{B_c^+ + B_c^-} + 2\sigma^{B_c^+ + B_c^{*-}} + \sigma^{B_c^{*+} + B_c^{*-}}$, we have

$$\sigma_{\rm LO}^{\rm FSS} = 7.67^{+0.55}_{-1.24} \times 10^{-1}\ \text{nb}, \qquad \sigma_{\rm NLO}^{\rm FSS} = 20.3^{+9.7}_{-4.9} \times 10^{-1}\ \text{nb}, \quad \text{for LHCb cuts;} \tag{35}$$

$$\sigma_{\rm LO}^{\rm FSS} = 4.32^{+1.14}_{-0.99} \times 10^{-3}\ \text{nb}, \qquad \sigma_{\rm NLO}^{\rm FSS} = 17.2^{+11.1}_{-5.7} \times 10^{-3}\ \text{nb}, \quad \text{for ATLAS cuts.} \tag{36}$$

The high-luminosity LHC (HL-LHC) will substantially increase the amount of proton-proton collisions delivered to the LHC experiments, with a planned integrated luminosity of 4000 fb^{-1} for ATLAS experiment [52], and 300 fb^{-1} for LHCb [53]. Assuming B_c is reconstructed through the decay $B_c^{\pm} \to J/\psi\pi^{\pm}$, whose branching fraction is predicted to be 0.5% [54], and J/ψ is reconstructed through $J/\psi \to l^+l^-(l = e, \mu)$ with a branching fraction of about 12% [45], the number of the reconstructed B_c-pair candidates is about 166–324 for LHCb experiment, and about 16–40 for ATLAS experiment.

C. Differential cross sections

As the number of events corresponding to LHCb experiment is promising, it is worthy to perform a more elaborate phenomenological analysis. The differential distributions in various variables with LHCb cuts are shown in Fig. 4, wherein, the LO and NLO predictions at $\mu_{R/F} = \mu_0$ are represented by dashed and solid lines respectively; the theoretical uncertainties, which are estimated by varying $\mu_{R/F}$ in the range $[\mu_0/2, 2\mu_0]$, are represented by color bands.

The distributions in M_{2B_c}, the invariant mass of the B_c-pair, are shown in Fig. 4(a). It can be seen that as M_{2B_c} increases from about 12 GeV to 32 GeV, both LO and NLO differential cross sections drop steadily. Although the NLO corrections are positive everywhere in the plotted M_{2B_c} range, the relative size of NLO corrections over LO contributions decreases with increasing M_{2B_c}.

The distributions in $|\Delta y|$, the absolute value of rapidity difference of the two B_c mesons, i.e., $|\Delta y| = |y_1 - y_2|$, are shown in Fig. 4(b). Similar to the M_{2B_c} distributions, the differential cross sections drop steadily with increasing $|\Delta y|$, and the NLO corrections are more significant in the small $|\Delta y|$ region.

The distributions in $p_{{\rm T},2B_c}$, the transverse momentum of the B_c-pair, are shown in Fig. 4(c). Since the B_c-pair with

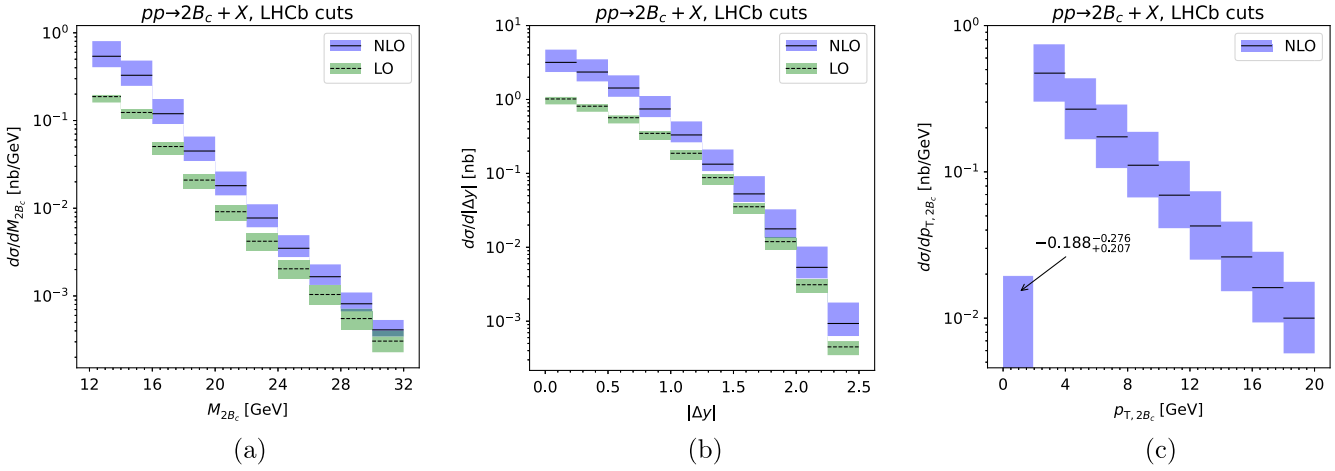

FIG. 4. The differential distributions in (a) the invariant mass of the B_c-pair M_{2B_c}, (b) the absolute value of rapidity difference of the B_c-pair $|\Delta y|$, (c) the transverse momentum of the B_c-pair $p_{{\rm T},2B_c}$.

nonvanishing $p_{T,2B_c}$ can only be produced in three-body processes, the second to the last bins only receive contribution from the $d\hat{\sigma}_{\text{real}}$ term of Eq. (16). For the first bin, the first term of Eq. (16) is negative, and larger in absolute value than the second term of Eq. (16). Hence the cross sections in the first bin can be negative at some energy scale. A resummation of the logarithms of $p^2_{T,2B_c}/s$ may help to solve this problem. This asks for a further investigation.

V. SUMMARY

In this work, we investigate the B_c-pair production in proton-proton collisions at the NLO accuracy in the framework of NRQCD factorization formalism. Various of S-wave B_c states, including configurations of $B_c^+ + B_c^-$, $B_c^+ + B_c^{*-}$, and $B_c^{*+} + B_c^{*-}$, are taken into account. The total cross sections and the differential cross sections versus various variables at the LHC with $\sqrt{s} = 14$ TeV are evaluated and presented in Table I and Fig. 4.

Numerical results show that, after including the NLO corrections, the total cross sections are significantly enhanced, and their dependences on renormalization and factorization scales are increased as well. We propose a potential explanation for the poor perturbative behavior, while further investigation is still needed. We also discuss the negative cross section problems encountered in the calculation.

Since B_c^* almost always decays to B_c, a prediction on B_c-pair candidates should sum over the $B_c^+ + B_c^-$, $B_c^+ + B_c^{*-}$, $B_c^{*+} + B_c^-$, and $B_c^{*+} + B_c^{*-}$ production rates. As a result, we obtain $\sigma^{\text{FSS}}_{\text{NLO}} = 2.03^{+0.97}_{-0.49}$ nb for LHCb experiment, and $\sigma^{\text{FSS}}_{\text{NLO}} = 1.72^{+1.11}_{-0.57} \times 10^{-2}$ nb for ATLAS experiment. Assuming B_c is reconstructed through $B_c^\pm \to J/\psi\pi^\pm$ and J/ψ is reconstructed through $J/\psi \to l^+l^-(l = e, \mu)$, the reconstructed B_c-pair candidates under the HL-LHC luminosity may reach 166–324 for LHCb experiment, and 16–40 for ATLAS experiment.

ACKNOWLEDGMENTS

This work was supported in part by the National Key Research and Development Program of China under Contract No. 2020YFA0406400, by the National Natural Science Foundation of China (NSFC) under Grants No. 11975236, No. 12175048, No. 12205061, and No. 12235008.

[1] G. T. Bodwin, E. Braaten, and G. Lepage, Phys. Rev. D **51**, 1125 (1995); **55**, 5853(E) (1997).
[2] A. Andronic, F. Arleo, R. Arnaldi, A. Beraudo, E. Bruna, D. Caffarri, Z. C. del Valle, J. G. Contreras, T. Dahms, A. Dainese *et al.*, Eur. Phys. J. C **76**, 107 (2016).
[3] J. P. Lansberg, Phys. Rep. **889**, 1 (2020).
[4] R. Aaij *et al.* (LHCb Collaboration), Phys. Lett. B **707**, 52 (2012).
[5] V. Khachatryan *et al.* (CMS Collaboration), J. High Energy Phys. 09 (2014) 094.
[6] V. Khachatryan *et al.* (CMS Collaboration), J. High Energy Phys. 05 (2017) 013.
[7] M. Aaboud *et al.* (ATLAS Collaboration), Eur. Phys. J. C **77**, 76 (2017).
[8] R. Aaij *et al.* (LHCb Collaboration), J. High Energy Phys. 06 (2017) 047; 10 (2017) 68.
[9] A. M. Sirunyan *et al.* (CMS Collaboration), Phys. Lett. B **808**, 135578 (2020).
[10] S. Acharya *et al.* (ALICE Collaboration), Phys. Rev. C **108**, 045203 (2023).
[11] R. Aaij *et al.* (LHCb Collaboration), J. High Energy Phys. 03 (2024) 088.
[12] R. Aaij *et al.* (LHCb Collaboration), arXiv:2311.15921.
[13] S. P. Baranov, Phys. Rev. D **55**, 2756 (1997).
[14] C. F. Qiao, L. P. Sun, and P. Sun, J. Phys. G **37**, 075019 (2010).
[15] R. Li, Y. J. Zhang, and K. T. Chao, Phys. Rev. D **80**, 014020 (2009).
[16] P. Ko, C. Yu, and J. Lee, J. High Energy Phys. 01 (2011) 070.
[17] C. H. Kom, A. Kulesza, and W. J. Stirling, Phys. Rev. Lett. **107**, 082002 (2011).
[18] A. V. Berezhnoy, A. K. Likhoded, and A. A. Novoselov, Phys. Rev. D **87**, 054023 (2013).
[19] A. P. Martynenko and A. M. Trunin, Phys. Rev. D **86**, 094003 (2012).
[20] Y. J. Li, G. Z. Xu, K. Y. Liu, and Y. J. Zhang, J. High Energy Phys. 07 (2013) 051.
[21] L. P. Sun, H. Han, and K. T. Chao, Phys. Rev. D **94**, 074033 (2016).
[22] A. M. Trunin and A. P. Martynenko, Proc. Sci. BaldinISH-EPPXXII (**2015**) 118.
[23] S. P. Baranov and A. H. Rezaeian, Phys. Rev. D **93**, 114011 (2016).
[24] A. K. Likhoded, A. V. Luchinsky, and S. V. Poslavsky, Phys. Rev. D **94**, 054017 (2016).
[25] Z. G. He and B. A. Kniehl, Phys. Rev. Lett. **115**, 022002 (2015).
[26] J. P. Lansberg, C. Pisano, F. Scarpa, and M. Schlegel, Phys. Lett. B **784**, 217 (2018); **791**, 420(E) (2019).
[27] Z. G. He, B. A. Kniehl, M. A. Nefedov, and V. A. Saleev, Phys. Rev. Lett. **123**, 162002 (2019).
[28] F. Scarpa, D. Boer, M. G. Echevarria, J. P. Lansberg, C. Pisano, and M. Schlegel, Eur. Phys. J. C **80**, 87 (2020).
[29] J. P. Lansberg, H. S. Shao, N. Yamanaka, Y. J. Zhang, and C. Noûs, Phys. Lett. B **807**, 135559 (2020).

[30] A. A. Prokhorov, A. V. Lipatov, M. A. Malyshev, and S. P. Baranov, Eur. Phys. J. C **80**, 1046 (2020).
[31] S. P. Baranov, A. V. Lipatov, and A. A. Prokhorov, Phys. Rev. D **106**, 034020 (2022).
[32] L. P. Sun and L. Sun, Chin. Phys. C **47**, 093105 (2023).
[33] Cong-Feng Qiao, Phys. Rev. D **66**, 057504 (2002).
[34] Z. G. He, B. A. Kniehl, and X. P. Wang, Phys. Rev. Lett. **121**, 172001 (2018).
[35] D. Kreimer, Phys. Lett. B **237**, 59 (1990).
[36] J. G. Korner, D. Kreimer, and K. Schilcher, Z. Phys. C **54**, 503 (1992).
[37] J. M. Campbell, F. Maltoni, and F. Tramontano, Phys. Rev. Lett. **98**, 252002 (2007).
[38] M. Butenschoen and B. A. Kniehl, Nucl. Phys. **B950**, 114843 (2020).
[39] T. Kinoshita, J. Math. Phys. (N.Y.) **3**, 650 (1962).
[40] T. D. Lee and M. Nauenberg, Phys. Rev. **133**, B1549 (1964).
[41] M. Beneke and V. A. Smirnov, Nucl. Phys. **B522**, 321 (1998).
[42] S. Catani and M. H. Seymour, Nucl. Phys. **B485**, 291 (1997); **B510**, 503(E) (1998).
[43] S. Catani, S. Dittmaier, M. H. Seymour, and Z. Trocsanyi, Nucl. Phys. **B627**, 189 (2002).
[44] T. J. Hou, J. Gao, T. J. Hobbs, K. Xie, S. Dulat, M. Guzzi, J. Huston, P. Nadolsky, J. Pumplin, C. Schmidt *et al.*, Phys. Rev. D **103**, 014013 (2021).
[45] P. A. Zyla *et al.* (Particle Data Group), Prog. Theor. Exp. Phys. **2020**, 083C01 (2020).
[46] E. J. Eichten and C. Quigg, Phys. Rev. D **49**, 5845 (1994).
[47] E. B. Gregory, C. T. H. Davies, I. D. Kendall, J. Koponen, K. Wong, E. Follana, E. Gamiz, G. P. Lepage, E. H. Muller, H. Na *et al.*, Phys. Rev. D **83**, 014506 (2011).
[48] R. Aaij *et al.* (LHCb Collaboration), Phys. Rev. Lett. **114**, 132001 (2015).
[49] M. Aaboud *et al.* (ATLAS Collaboration), Phys. Rev. D **104**, 012010 (2021).
[50] A. M. Sirunyan *et al.* (CMS Collaboration), Phys. Rev. D **102**, 092007 (2020).
[51] A. Colpani Serri, Y. Feng, C. Flore, J. P. Lansberg, M. A. Ozcelik, H. S. Shao, and Y. Yedelkina, Phys. Lett. B **835**, 137556 (2022).
[52] S. Sanchez Cruz (CMS Tracker Group), Proc. Sci. ICHEP2022 (**2022**) 637.
[53] S. Kholodenko (LHCb ECAL UII Working Group), Proc. Sci. PANIC2021 (**2022**) 100.
[54] C. H. Chang and Y. Q. Chen, Phys. Rev. D **49**, 3399 (1994).